ined the binding of BiP with a DnaJ-domain mutant of ERdj5 in which histidine 63 in the HPD motif is replaced with glutamine (ERdj5/H63Q) (*13*). ERdj5/H63Q did not bind to BiP, even in the presence of ATP (Fig. 4A). Thus, ERdj5 interacts through its DnaJ domain with BiP.

We examined the in vivo effect of the ERdj5/H63Q mutant on HMW complex formation and on the ERAD of J chains. Accumulation of the J chain HMW complex was considerably decreased 48 hours after transfection with wild-type ERdj5 compared with amounts after mock transfection (Fig. 4B). In contrast, neither transfection with ERdj5/H63Q nor with the ERdj5/SS mutant repressed the accumulation of J chain HMW complexes. Transfection with the ERdj5/H63Q mutant did not accelerate J-chain degradation (Fig. 4C and fig. S3) even though this mutant retains the disulfide reductase activity (fig. S2). Thus, both the reductase activity of ERdj5, which is conferred by its CXXC motifs, and the association of ERdj5 with the molecular chaperone BiP are necessary to prevent multimer formation by the misfolded proteins and also to promote efficient ERAD of such proteins.

We next examined the involvement of ERdj5 in the EDEM-mediated ERAD pathway. EDEM coimmunoprecipitated with both wild-type ERdj5 and the ERdj5/AA mutant in HEK293 cells, which suggests that the binding of EDEM with ERdj5 is CXXC-independent (fig. S8). Acceleration of ERAD by EDEM overexpression is dependent on mannose-trimming and is inhibited by kifunensine, an inhibitor of ER mannosidase I (*3*). Promotion of ERAD by ERdj5 overexpression was totally abolished in the presence of kifunensine (Fig. 4D), which suggests that ERdj5-mediated ERAD requires EDEM to function.

Thus, ERdj5, either overexpressed or endogenous, can serve as a key component for the ERAD of misfolded proteins. The following are all required for ERdj5-mediated ERAD acceleration: (i) the reductase activity of ERdj5, which is conveyed through its CXXC motif; (ii) the binding of ERdj5, through its DnaJ domain, to the ER-resident Hsp70 family chaperone BiP; and (iii) the functional interaction of ERdj5 with EDEM, a lectin-like molecule that may recognize the Man_8 *N*-glycan on misfolded proteins to be degraded. ERdj5-mediated cleavage of intermolecular disulfide bridges decreased the accumulation of covalent multimeric forms of misfolded proteins in the ER; such accumulations are expected to hinder the retrograde transport of misfolded proteins through the retrotranslocation channel. ERdj5 may prevent disulfide-linked aggregation and/or misfolding of substrates by maintaining them in reduced states and may enhance their ERAD by increasing retrotranslocation-competent misfolded proteins.

The redox potential of ERdj5 is even more reducing than the ER redox status (*16*) or the redox potential of PDI (*17*). ERdj5 has three CXPC motifs, consistent with reports that the redox potential of CXPC motifs contained in thioredoxin superfamily proteins is reducing (*18*). Its reducing redox potential indicates that ERdj5 is thermodynamically stable in an oxidized form in the ER redox environment and that ERdj5 can function as a strong disulfide reductase once it accepts electrons from electron donors. Electrons might be transported into the ER from the reducing cytosol or provided from the high ER concentration of the reduced form of nicotinamide adenine dinucleotide phosphate (NADPH) (*19*). These possibilities remain to be addressed.

Here, we have established the presence of a supramolecular functional ERAD complex, comprising EDEM, ERdj5, and BiP, which have distinct, but linked and concerted, roles (fig. S9). In this model, after the transfer of terminally misfolded proteins from calnexin to EDEM, ERdj5 bound to EDEM cleaves their disulfide bonds, which results in dissociation of the covalent multimeric substrates. At the same time, ERdj5 activates the conversion of the ATP-form of BiP to adenosine diphosphate form, resulting in dissociation of BiP from ERdj5, which, in turn, strongly binds the substrates (*20*) and holds them in a dislocation-competent state until they are transferred to the retrotranslocation channel.

References and Notes

1. L. Ellgaard, A. Helenius, *Nat. Rev. Mol. Cell Biol.* **4**, 181 (2003).
2. K. Kanehara, S. Kawaguchi, D. T. Ng, *Semin. Cell Dev. Biol.* **18**, 743 (2007).
3. N. Hosokawa *et al.*, *EMBO Rep.* **2**, 415 (2001).
4. Y. Oda, N. Hosokawa, I. Wada, K. Nagata, *Science* **299**, 1394 (2003).
5. M. Molinari, V. Calanca, C. Galli, P. Lucca, P. Paganetti, *Science* **299**, 1397 (2003).
6. Y. Oda *et al.*, *J. Cell Biol.* **172**, 383 (2006).
7. N. Hosokawa, I. Wada, Y. Natsuka, K. Nagata, *Genes Cells* **11**, 465 (2006).
8. A. Mezghrani *et al.*, *EMBO J.* **20**, 6288 (2001).
9. D. Tortorella *et al.*, *J. Cell Biol.* **142**, 365 (1998).
10. Materials and methods are available as supporting material on *Science* Online.
11. S. Pollock *et al.*, *EMBO J.* **23**, 1020 (2004).
12. P. M. Cunnea *et al.*, *J. Biol. Chem.* **278**, 1059 (2003).
13. A. Hosoda, Y. Kimata, A. Tsuru, K. Kohno, *J. Biol. Chem.* **278**, 2669 (2003).
14. Y. Shen, L. M. Hendershot, *Mol. Biol. Cell* **16**, 40 (2005).
15. L. Ellgaard, L. W. Ruddock, *EMBO Rep.* **6**, 28 (2005).
16. C. Hwang, A. J. Sinskey, H. F. Lodish, *Science* **257**, 1496 (1992).
17. N. J. Darby, T. E. Creighton, *Biochemistry* **34**, 16770 (1995).
18. G. Roos *et al.*, *J. Mol. Biol.* **368**, 800 (2007).
19. S. Piccirella *et al.*, *J. Biol. Chem.* **281**, 4671 (2006).
20. K. Liberek, D. Skowyra, M. Zylicz, C. Johnson, C. Georgopoulos, *J. Biol. Chem.* **266**, 14491 (1991).

21. We thank N. Hosokawa for providing NHK and the EDEM protein plasmids. We also thank R. I. Morimoto and K. Inaba for critical discussions and advice. This work was supported by Grants-in-Aid for Creative Scientific Research (19GS0314) and Scientific Research (19058008) (to K.N.) and the Canadian Institutes of Health Research (to D.Y.T.). R.U. was supported by a fellowship from the Japan Society for the Promotion of Science.

Supporting Online Material

www.sciencemag.org/cgi/content/full/321/5888/569/DC1
Materials and Methods
Figs. S1 to S9
References

18 April 2008; accepted 12 June 2008
10.1126/science.1159293

The Crystal Structure of [Fe]-Hydrogenase Reveals the Geometry of the Active Site

Seigo Shima,[1]*† Oliver Pilak,[1]* Sonja Vogt,[1] Michael Schick,[1] Marco S. Stagni,[2] Wolfram Meyer-Klaucke,[2] Eberhard Warkentin,[3] Rudolf K. Thauer,[1] Ulrich Ermler[3]†

Biological formation and consumption of molecular hydrogen (H_2) are catalyzed by hydrogenases, of which three phylogenetically unrelated types are known: [NiFe]-hydrogenases, [FeFe]-hydrogenases, and [Fe]-hydrogenase. We present a crystal structure of [Fe]-hydrogenase at 1.75 angstrom resolution, showing a mononuclear iron coordinated by the sulfur of cysteine 176, two carbon monoxide (CO) molecules, and the sp^2-hybridized nitrogen of a 2-pyridinol compound with back-bonding properties similar to those of cyanide. The three-dimensional arrangement of the ligands is similar to that of thiolate, CO, and cyanide ligated to the low-spin iron in binuclear [NiFe]- and [FeFe]-hydrogenases, although the enzymes have evolved independently and the CO and cyanide ligands are not found in any other metalloenzyme. The related iron ligation pattern of hydrogenases exemplifies convergent evolution and presumably plays an essential role in H_2 activation. This finding may stimulate the ongoing synthesis of catalysts that could substitute for platinum in applications such as fuel cells.

Molecular hydrogen (H_2) is a relatively inert molecule. The dissociation energy of the H-H bond is 436 kJ mol^{-1}, and its pK_a is 35 (*1*, *2*). Despite this, H_2 is used or produced by many microorganisms in their energy metabolism. Indeed, H_2 was one of the earliest energy sources available on Earth when life evolved. H_2/H^+ interconversion reactions ($H_2 \leftrightharpoons 2H^+ + 2e^-$) are catalyzed by hydrogenases that contain nickel and/or iron as key components in their active sites; these hydrogenases are more efficient catalysts than platinum, which is used industrially to catalyze hydrogenation. H_2 is considered a major fuel in future energy technology, but the amounts of catalyst required for large-scale H_2 production and use will require alternatives to platinum, which is expensive and not abundant. One approach of current research is to learn from hydrogenases (Fig. 1), and model compounds mimicking the metal centers of hydro-

genase have recently been synthesized that can interact with protons and/or H_2 (*3*–*7*).

The most prominent hydrogenases are [NiFe]-hydrogenase (in bacteria and archaea) and [FeFe]-hydrogenase (in bacteria and eukaryotes) (*8*). The structures of their binuclear metal active sites are pictured in Fig. 1, A and B (*9*–*17*). In addition to the binuclear metal center, both types of hydrogenases harbor at least one essential [4Fe-4S] cluster. The iron in the binuclear [NiFe] center (Fig. 1A) is redox-inactive and low-spin (*18*), as probably is the iron proximal to the [4Fe-4S] cluster in the binuclear [FeFe] center (*19*) (Fig. 1B). The third type of hydrogenases, the [Fe]-hydrogenase—formerly named iron-sulfur cluster–free hydrogenase or H_2-forming methylenetetrahydromethanopterin (methylene-H_4MPT) dehydrogenase (*20*)—contains a mononuclear iron center (Fig. 1C) and is found only in some hydrogenotrophic methanogenic archaea, where it catalyzes one step involved in CO_2 reduction to methane (Fig. 2). Each subunit of the homodimeric enzyme contains one iron (which is not redox-active) and no iron-sulfur clusters.

In [Fe]-hydrogenase, the iron center is the catalytically active constituent of an iron guanylyl pyridone cofactor (FeGP cofactor), which can be extracted from the enzyme by denaturation in the presence of mercaptoethanol and used for reconstitution of the active enzyme from inactive heterologously produced apoenzyme (*21*). The FeGP cofactor is light- and temperature-sensitive (*22*), which hampers purification to homogeneity. Observed decomposition products are guanylyl pyridone (see below), two CO molecules, and one iron ion (*23*). Infrared (IR) spectroscopic analysis (*24*) revealed two CO molecules as iron ligands; x-ray absorption analysis (*25*) predicted two CO, one sulfur, and one or two N/O ligands at coordination distance to iron; Mössbauer spectroscopic data (*26*) identified the iron as low spin, either in the Fe(0) or Fe(II) oxidation state; and x-ray structure analysis of the [Fe]-hydrogenase without the FeGP cofactor (apoenzyme) established the overall architecture of the enzyme (*27*) (Fig. 3). Here, we describe the structure of the [Fe]-hydrogenase–FeGP complex (holoenzyme) at 1.75 Å resolution (Fig. 3A) (*28*). This allows a detailed three-dimensional view of the structure and binding of the intact FeGP cofactor—the site of H_2 activation—and thereby integrates previous biochemical and biophysical data into a comprehensive and consistent picture.

To elucidate the holoenzyme structure, we reconstituted the heterologously produced apoenzyme of *Methanocaldococcus jannaschii* with the labile FeGP cofactor under completely anaerobic and red-light conditions and crystallized the reconstituted enzyme. The crystal structure of [Fe]-hydrogenase contains the FeGP cofactor with a high occupancy embedded in front of the C-terminal end of the parallel β sheet of both Rossmann fold–like peripheral units and capped by an α-helical subdomain (Fig. 3). The specific amino acid residues involved in binding of the FeGP cofactor to the enzyme are shown in fig. S1. The guanosine monophosphate moiety functions to anchor the FeGP cofactor, and its binding mode essentially corresponds to the adenosine monophosphate moiety of dinucleotide binding proteins (Fig. 4). The catalytically relevant iron-center moiety is located close to the intersubunit clefts (Fig. 3) and consists of a mononuclear iron atom surrounded by a distorted square pyramidal or an octahedral ligation shell dependent on the enzymatic state (Fig. 5).

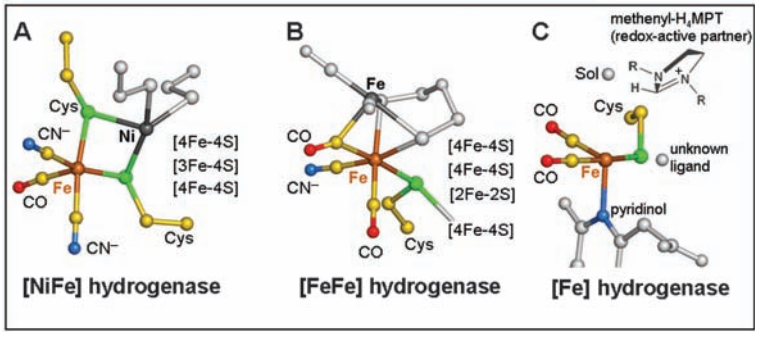

Fig. 1. Superimposed active-site structure of the three phylogenetically unrelated hydrogenases. (**A**) [NiFe]-hydrogensase from *Desulfovibrio gigas* (*9*, *12*). (**B**) [FeFe]-hydrogenase from *Clostridium pasteurianum* (*13*) and *Desulfovibrio desulfuricans* (*14*, *16*). (**C**) [Fe]-hydrogenase from *Methanocaldococcus jannaschii* (this work). In [Fe]-hydrogenase, the fifth and sixth ligation sites are marked by gray spheres. All three hydrogenase types have in common a low-spin iron (brown) ligated by thiolate(s), CO, and cyanide or pyridinol (considered as cyanide functional analog), which acts together with a redox-active partner (dark gray). The partners—Ni, the distal iron, and methenyl-H_4MPT^+ (modeled), respectively—take over the electrons or the hydride and perhaps play a role in the heterolytic cleavage of H_2.

Fig. 2. Reaction catalyzed by [Fe]-hydrogenase in methanogenic archaea. The heterolytic cleavage of H_2 by the enzyme is dependent on the presence of methenyl-H_4MPT^+, whose methenyl C14a has carbocation character and is therefore an excellent hydride acceptor. H_4MPT, tetrahydromethanopterin.

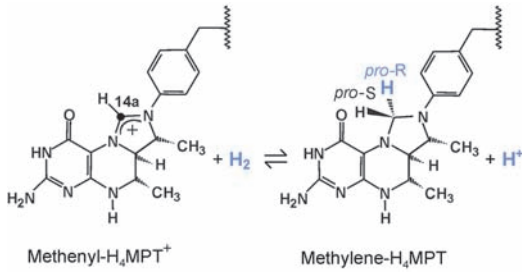

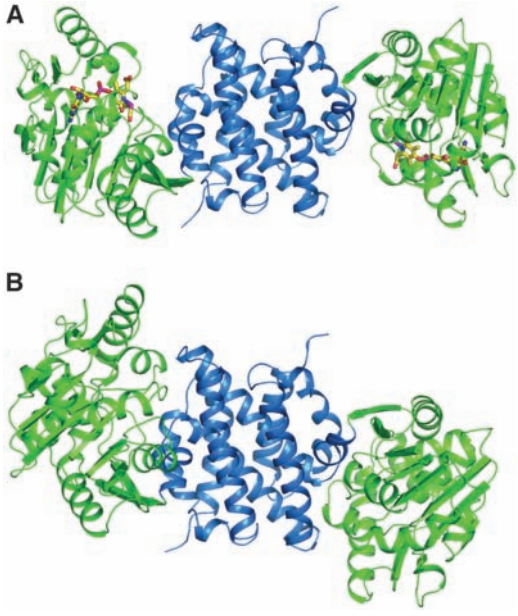

Fig. 3. Ribbon diagrams of the [Fe]-hydrogenase of *M. jannaschii*. The homodimeric enzyme is composed of three folding units. The two peripheral units (N-terminal segments) consist of a Rossmann fold–like domain (green) which can be further subdivided into a classical Rossmann fold, an extension (βαβ), and an α-helical insertion region. The unique central unit (in blue) constitutes an intertwined helix bundle formed by the C-terminal segments of both subunits (*27*). The structure of the holoenzyme (**A**) is in an open conformation and that of the apoenzyme (**B**) is in a closed conformation with respect to the cleft between the central and the peripheral units (*27*). The rotation angle between the states is 37°. The FeGP cofactor is bound to the peripheral units and is depicted as a color-coded stick model.

[1]Max-Planck-Institut für Terrestrische Mikrobiologie and Laboratorium für Mikrobiologie, Fachbereich Biologie, Philipps-Universität Marburg, Karl-von-Frisch-Straße, D-35043 Marburg, Germany. [2]EMBL Hamburg, Notkestr. 85, D-22603 Hamburg, Germany. [3]Max-Planck-Institut für Biophysik, Max-von-Laue-Straße 3, D-60438 Frankfurt/Main, Germany.

*These authors contributed equally to this work.
†To whom correspondence should be addressed. E-mail: ulermler@mpibp-frankfurt.mpg.de; shima@mpi-marburg.mpg.de

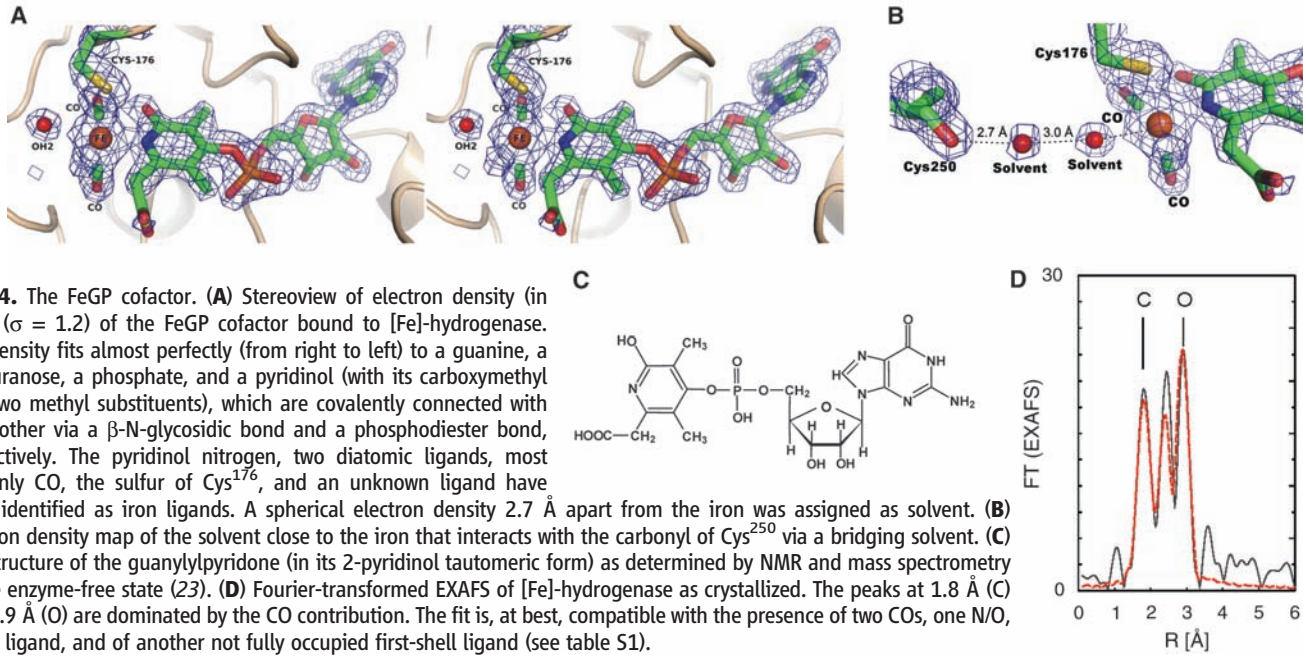

Fig. 4. The FeGP cofactor. (**A**) Stereoview of electron density (in blue) (σ = 1.2) of the FeGP cofactor bound to [Fe]-hydrogenase. The density fits almost perfectly (from right to left) to a guanine, a ribofuranose, a phosphate, and a pyridinol (with its carboxymethyl and two methyl substituents), which are covalently connected with each other via a β-N-glycosidic bond and a phosphodiester bond, respectively. The pyridinol nitrogen, two diatomic ligands, most certainly CO, the sulfur of Cys^{176}, and an unknown ligand have been identified as iron ligands. A spherical electron density 2.7 Å apart from the iron was assigned as solvent. (**B**) Electron density map of the solvent close to the iron that interacts with the carbonyl of Cys^{250} via a bridging solvent. (**C**) The structure of the guanylylpyridone (in its 2-pyridinol tautomeric form) as determined by NMR and mass spectrometry in the enzyme-free state (*23*). (**D**) Fourier-transformed EXAFS of [Fe]-hydrogenase as crystallized. The peaks at 1.8 Å (C) and 2.9 Å (O) are dominated by the CO contribution. The fit is, at best, compatible with the presence of two COs, one N/O, one S ligand, and of another not fully occupied first-shell ligand (see table S1).

One iron ligand is the pyridinol nitrogen atom, which links the organic guanylylpyridinol molecule with the iron center (Fig. 4). The hydroxylate and carboxylate substituents of pyridinol are not used as iron ligands, although the latter is partly disordered and must be analyzed with caution. Because of its planarity, the heterocyclic ring is present in a pyridinol and not in a pyridone tautomeric form (Fig. 4C), and therefore the nitrogen atom is in a π-accepting sp^2 configuration. The pyridinol group—in particular, if the hydroxyl group is in a deprotonated state—might have ligand back-bonding properties similar to those of cyanide (*29*, *30*), which acts as an iron ligand in the [NiFe]- and [FeFe]-hydrogenases. Further ligands are two CO molecules that are optimally accommodated between several nonpolar atoms of the polypeptide chain. The CO molecules form an angle of 90°, in agreement with the interpretation of the IR spectrum of the holoenzyme (*24*). The sole proteinaceous ligand originates from the thiolate sulfur of Cys^{176} that points toward the iron from a loop following strand 169:174 at the bottom of the intersubunit cleft.

The chemical nature of the fifth ligand is unknown, and its electron density cannot definitely be assigned as a monatomic or diatomic ligand, although it is clearly connected with that of the iron and of relatively high occupancy (i.e., corresponds to a completely occupied water molecule). The electron density (σ = 1.2) at the position of the unknown ligand (fig. S2) is increased (by a factor of 1.6) after soaking of the crystals with 3 mM cyanide, which suggests that this is the binding site of the reversible and noncompetitive inhibitor cyanide (*22*).

The vacant sixth coordination site of the iron contains a spherical electron density interpreted as a monatomic solvent molecule (i.e., a completely occupied water molecule) that is, however, at a distance of 2.7 Å too far away to be considered as a ligand (Fig. 4). We predict this site to be the binding position of extrinsic CO (Fig. 5) known to inhibit [Fe]-hydrogenase, as the Fourier-transformed IR spectrum of the CO inhibited enzyme predicts a perpendicular orientation of the extrinsic CO relative to the two intrinsic COs (*24*). Because CO is a competitive inhibitor with respect to H_2, the latter most likely also binds to this site (Figs. 1 and 5). The solvent close to the iron interacts with a second solvent molecule, which in turn is linked to the carbonyl group of the strictly conserved Cys^{250} (Fig. 4A). Interestingly, the Cys^{250} → Ala mutant shows reduced enzyme activity (table S2).

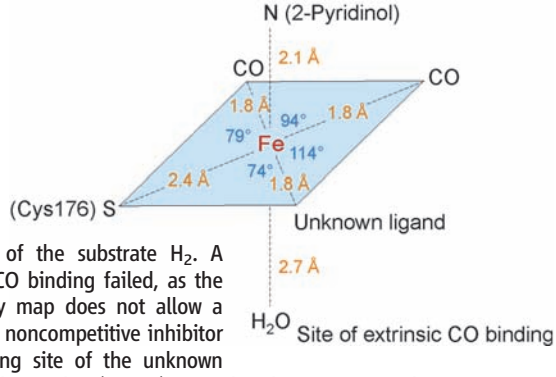

Fig. 5. Coordination of the iron in the active site of [Fe]-hydrogenase. The iron sits in the plane of the square spanned by the Cys^{176} sulfur, two COs, and the unknown ligand; the nitrogen is at the top of the pyramid. The sixth ligation site trans to the pyridinol nitrogen is presumably the binding site of the competitive inhibitor CO (according to IR spectroscopy data) and of the substrate H_2. A structural confirmation of the extrinsic CO binding failed, as the quality of the resulting electron density map does not allow a distinction between a water and CO. The noncompetitive inhibitor cyanide presumably occupies the binding site of the unknown ligand as derived from x-ray crystallographic studies (fig. S2). Note that the iron, one of the intrinsic COs, the unknown ligand (or the cyanide), and probably the extrinsic CO are located in the plane of the pyridinol ring. The distances and angles between the irons and ligands are drawn in, except for those between the four ligands in the plane and the pyridinol's nitrogen and the nearby solvent assigned as water [N/S, 86°; N/CO (left), 102°; N/CO (right), 91°; N/cyanide, 94°; H_2O/S, 90°; H_2O/CO (left), 72°; H_2O/CO (right), 91°; H_2O/cyanide, 90°]. The distances between iron and the four identifiable ligands agree well with those determined in parallel by EXAFS spectroscopy (Fig. 4C and table S1).

A comparison of the active-site metal centers of the three hydrogenase types reveals unexpected common features (Fig. 1) previously recognized for the two binuclear hydrogenases. All three types contain a redox-inactive low-spin iron, presumably in the oxidation state II, that is asymmetrically ligated by five or six ligands arranged as a distorted square pyramid or octahedron. Moreover, three π-accepting ligands comprising CO, cyanide, or pyridinol (considered as a cyanide functional analog) are oriented perpendicular to each other in a geometrically related manner, and a thiolate sulfur always coordinates the iron trans to a diatomic molecule (Fig. 1). All three iron centers act together with a redox-active partner—methenyl-H_4MPT^+ in the case of [Fe]-hydrogenase, the distal iron in the case of [FeFe]-hydrogenase, and nickel in the case of [NiFe] hydrogenase—whose spatial position relative to the other ligands is also similar. Apparently, these related iron centers, with unusual nonproteinaceous ligands thought to be synthesized by three different enzymatic machineries (*31*) and embedded into three architecturally different hydro-

genase structures, evolved independently. Remarkably, hydrogenases are the only metalloenzymes that use toxic CO and cyanide (or pyridinol) as metal ligands. Thus, hydrogenases are an impressive example of convergent evolutionary development as a consequence of specific biological and/or chemical restraints. However, the intrinsic physicochemical properties of the unique iron ligation pattern are not yet understood, nor are their implications for the technologically important H_2 activation reaction.

Despite the related low-spin iron centers, the enzymatic mechanism of [Fe]-hydrogenase differs fundamentally from that of the other types because of the different nature of the redox-active partner and the accompanying electron delivery mode. In [NiFe]- and [FeFe]-hydrogenases, the electrons of H_2 reduction flow one by one through the redox-active metals and several iron-sulfur clusters over a large distance to an electron acceptor. The active-site structures essentially remain fixed during H_2 cleavage, and H_2 reaches the deeply buried active site by a long diffusion channel. In [Fe]-hydrogenase, however, the found ternary reaction mechanism and the exchange between H_2 and protons of water solely in the presence of methenyl-H_4MPT$^+$ (*32*) (see partial structure in Fig. 2) suggests that methenyl-H_4MPT$^+$ directly accepts the hydride from H_2. This conclusion is supported by the x-ray structure, as the cleft between the peripheral and central units can accommodate the bulky methenyl-H_4MPT$^+$ molecule and the C14a atom can be positioned sufficiently close to the iron without causing severe clashes with the polypeptide chain (fig. S3). Because the intersubunit cleft in the holoenzyme is, in fact, too large for an optimal methenyl-H_4MPT$^+$ adjustment, we assume that its binding is accompanied by an induced-fit movement constituting the catalysis-competent active-site before each turnover. The expected large-scale conformational changes are reflected in the different positions of the peripheral unit relative to the central unit found in the structures of the holo- and apoenzymes (Fig. 3), mainly induced by crystal forces. H_2 can readily reach the solvent-exposed Fe center, which is probably encapsulated upon methenyl-H_4MPT$^+$ binding.

The most attractive hypothesis for the mechanism of H_2 cleavage in [Fe]-hydrogenases is based on a concerted action of the strong hydride acceptor methenyl-H_4MPT$^+$ and the Lewis acid Fe(II) that lowers the pK_a value of H_2, preferably when bound in a side-on conformation. The polarized H_2 ligated to the postulated binding site (Fig. 5) is attacked from the adjacent carbocation C14a of methenyl-H_4MPT$^+$ from the *Re*-face of the ring system (see Fig. 2), generating methylene-H_4MPT. Acceptors for the released proton within 6.5 Å from the iron include the Cys^{176} thiolate ligand, the pyridinol nitrogen, oxygen, and carboxyl oxygen as well as two conserved histidines, His^{14} and His^{201} (for the position of the two histidines relative to the iron, see fig. S1B). A His^{14} → Ala mutation drastically reduces the hydrogenase activity of the enzyme, whereas His^{201} → Ala has only a minor effect (table S2).

Although there are still many questions to be answered, the crystal structure allows us to draw the following conclusions: (i) The active-site iron is definitely mononuclear, not dinuclear as in the [FeFe]- and [NiFe]-hydrogenases. (ii) The presented structural data, together with results of studies using various spectroscopic methods [nuclear magnetic resonance (NMR), mass, IR, Mössbauer, and extended x-ray absorption fine structure (EXAFS) (*23*–*26*)] and information from mutational analysis (*25*), converge to a coherent result. (iii) The structures of the [Fe]-, [FeFe]-, and [NiFe]-hydrogenases are completely different but share features in their active site that can only have evolved convergently (Fig. 1). (iv) The detailed three-dimensional structure will allow density functional theory (DFT) calculations of energy profiles, which will help to exclude some of the proposed mechanisms of H_2 activation. (v) Model complexes can be constructed on the basis of the iron center of [Fe]-hydrogenase, and their analysis will provide further insight into its essential but not yet understood function in H_2 activation (*3*–*7*).

References and Notes

1. D. M. Heinekey, W. J. Oldham, *Chem. Rev.* **93**, 913 (1993).
2. G. J. Kubas, *Catal. Lett.* **104**, 79 (2005).
3. C. Tard *et al.*, *Nature* **433**, 610 (2005).
4. T. Liu, M. Y. Darensbourg, *J. Am. Chem. Soc.* **129**, 7008 (2007).
5. A. K. Justice *et al.*, *Inorg. Chem.* **46**, 1655 (2007).
6. S. Ogo *et al.*, *Science* **316**, 585 (2007).
7. X. Hu, B. S. Brunschwig, J. C. Peters, *J. Am. Chem. Soc.* **129**, 8988 (2007).
8. P. M. Vignais, B. Billoud, J. Meyer, *FEMS Microbiol. Rev.* **25**, 455 (2001).
9. A. Volbeda *et al.*, *Nature* **373**, 580 (1995).
10. E. Garcin *et al.*, *Structure* **7**, 557 (1999).
11. H. Ogata *et al.*, *J. Am. Chem. Soc.* **124**, 11628 (2002).
12. A. Volbeda *et al.*, *J. Biol. Inorg. Chem.* **10**, 239 (2005).
13. J. W. Peters, W. N. Lanzilotta, B. J. Lemon, L. C. Seefeldt, *Science* **282**, 1853 (1998).
14. Y. Nicolet, C. Piras, P. Legrand, C. E. Hatchikian, J. C. Fontecilla-Camps, *Structure* **7**, 13 (1999).
15. B. J. Lemon, J. W. Peters, *Biochemistry* **38**, 12969 (1999).
16. Y. Nicolet *et al.*, *J. Am. Chem. Soc.* **123**, 1596 (2001).
17. Z. Chen *et al.*, *Biochemistry* **41**, 2036 (2002).
18. M. Frey, *ChemBioChem* **3**, 153 (2002).
19. A. Silakov, E. J. Reijerse, S. P. J. Albracht, E. C. Hatchikian, W. Lubitz, *J. Am. Chem. Soc.* **129**, 11447 (2007).
20. S. Shima, R. K. Thauer, *Chem. Rec.* **7**, 37 (2007).
21. G. Buurman, S. Shima, R. K. Thauer, *FEBS Lett.* **485**, 200 (2000).
22. E. J. Lyon *et al.*, *Eur. J. Biochem.* **271**, 195 (2004).
23. S. Shima *et al.*, *Angew. Chem. Int. Ed.* **43**, 2547 (2004).
24. E. J. Lyon *et al.*, *J. Am. Chem. Soc.* **126**, 14239 (2004).
25. M. Korbas *et al.*, *J. Biol. Chem.* **281**, 30804 (2006).
26. S. Shima, E. J. Lyon, R. K. Thauer, B. Mienert, B. Bill, *J. Am. Chem. Soc.* **127**, 10430 (2005).
27. O. Pilak *et al.*, *J. Mol. Biol.* **358**, 798 (2006).
28. See supporting material on *Science* Online.
29. J. M. Rawson, R. E. P. Winpenny, *Coord. Chem. Rev.* **139**, 313 (1995).
30. S. Wolfe, N. Weinberg, Y. Hsieh, *Theor. Chem. Acc.* **118**, 265 (2007).
31. A. Böck, P. W. King, M. Blokesch, M. C. Posewitz, *Adv. Microb. Physiol.* **51**, 1 (2006).
32. S. Vogt, E. J. Lyon, S. Shima, R. K. Thauer, *J. Biol. Inorg. Chem.* **13**, 97 (2008).

33. Supported by the Max Planck Society, the Fonds der Chemischen Industrie, and the Bundesministerium für Bildung und Forschung (BioH$_2$ project). We thank H. Michel for continuous support, and the staff of beamline PXII at the Swiss Light Source for help during data collection. Coordinates of [Fe]-hydrogenase and [Fe]-hydrogenase complexed with cyanide have been deposited in the Research Collaboratory for Structural Bioinformatics Protein Data Bank under accession codes 3DAG and 3DAF.

Supporting Online Material

www.sciencemag.org/cgi/content/full/321/5888/572/DC1
Materials and Methods
Figs. S1 to S3
Tables S1 to S3
References

10 April 2008; accepted 5 June 2008
10.1126/science.1158978

Manipulating the Metazoan Mitochondrial Genome with Targeted Restriction Enzymes

Hong Xu, Steven Z. DeLuca, Patrick H. O'Farrell*

High copy number and random segregation confound genetic analysis of the mitochondrial genome. We developed an efficient selection for heritable mitochondrial genome (mtDNA) mutations in *Drosophila*, thereby enhancing a metazoan model for study of mitochondrial genetics and mutations causing human mitochondrial disease. Targeting a restriction enzyme to mitochondria in the germline compromised fertility, but escaper progeny carried homoplasmic mtDNA mutations lacking the cleavage site. Among mutations eliminating a site in the cytochrome c oxidase gene, *mt:CoI*^{A302T} was healthy, *mt:CoI*^{R301L} was male sterile but otherwise healthy, and *mt:CoI*^{R301S} exhibited a wide range of defects, including growth retardation, neurodegeneration, muscular atrophy, male sterility, and reduced life span. Thus, germline expression of mitochondrial restriction enzymes creates a powerful selection and has allowed direct isolation of mitochondrial mutants in a metazoan.

A typical animal cell contains hundreds to thousands of copies of the mitochondrial genome (mtDNA), which encodes 13 essential subunits of the electron transport chain complexes and RNAs (2 rRNAs and 22 tRNAs) required for mitochondrial translation (*1*, *2*). It is not clear how the genetic integrity of this amitotically distributed genome is main-